Lu, Liangliang; Kujala, Pentti; Valdez Banda, Osiris; Goerlandt, Floris

Ramming induced ice loads between the ship bow and multiyear thick ice in Antarctic Weddell Sea

Published in:
Developments in the Collision and Grounding of Ships and Offshore Structures

Published: 01/01/2020

Document Version
Peer-reviewed accepted author manuscript, also known as Final accepted manuscript or Post-print

Please cite the original version:
Lu, L., Kujala, P., Valdez Banda, O., & Goerlandt, F. (2020). Ramming induced ice loads between the ship bow and multiyear thick ice in Antarctic Weddell Sea. In C. Guedes Soares (Ed.), *Developments in the Collision and Grounding of Ships and Offshore Structures: Proceedings of the 8th International Conference on Collision and Grounding of Ships and Offshore Structures, ICCGS 2019* (pp. 204-211). (Proceedings in Marine Technology and Ocean Engineering; Vol. 4). CRC Press.

Ramming induced ice loads between the ship bow and multiyear thick ice in Antarctic Weddell Sea

L. Lu, P. Kujala, O. A. Valdez Banda
Aalto University, Finland

F. Gerlandt
Dalhousie University, Halifax, Canada

ABSTRACT: The Polar regions are increasingly in focus in recent years. Both the Antarctic and Arctic sea areas are receiving more and more ship visits. Therefore, understanding ship-ice interaction and ice loads, especially with thick ice, is a vital step to avoid possibly disastrous accidents and environmental damages to these sensitive regions. This paper is based on a particular case in Weddell Sea Expedition 2019, where the ship continuously carves thick multiyear thick ice to recover an AUV under the ice floe. The ship is instrumented with in-built strain gauges at the bow, bow shoulder and stern shoulder with a monitoring camera above the instrumented panels. In addition, ship navigation and machine control parameters, including ship speed, rudder angle and power are also recorded by the central measurement unit. This paper aims to present the measured ramming-induced ice loads with thick ice and apply statistical method to analyze all the relevant parameters to provide insights into possible factors or operations leading to high ice loads.

1 INTRODUCTION AND BACKGROUND

The focuses on the Polar Regions are increasing gradually in recent years. Both the Antarctic and Arctic sea areas are receiving more and more ship visits. The interest to Arctic region is due primarily to the presence of natural resources (Frédéric, 2011), potential shipping routes, and tourism. Navigation activities in Antarctic initiated relatively long ago, starting from the explorations and fishing activities. Then, polar research and supply visits increased as well, as scientific interest in the Antarctic increased. Nowadays, tourism is also a quite popular activity and increases yearly. Ships entering into polar waters are very likely to meet ice conditions in various circumstances. Additionally, the low temperature also requires higher-class steel and structure (Bridge et al., 2018). Therefore, understanding the ice loads on the ship hull during the ship-ice interaction process is very important. It is also a vital step to avoid the unnecessary ice impact damage and further environmental damages to the sensitive regions.

The methods to study the loads on the ship structure include numerical approaches, laboratory experiments and full-scale measurements. They all have their limitations, however full-scale measurement is considered to have the advantage that all the variations, e.g. in ice conditions and the ice-breaking process, are embedded in the measurements (Suominen, 2018). The approaches applied to measure ice-induced loads in full scale are concluded into two main categories: indirect structural strain measurements and direct measurements of the contact pressure or load (Suominen, 2018; Kendrick and Daley, 2011; and Ehlers et al., 2015). The measurements in this paper are based on the shear strain difference, which are considered as the least sensitive to the load height and locations (Suominen, 2018).

The full-scale ice loading measurements have been studied in many perspectives. There are researches on the statistics (Kujala, 1994; Jordaan et al., 1993), on local design pressure (Taylor et al., 2010; Jordaan et al. 2010), on the uncertainties about the full-scale measurements (Suominen, 2018), on finding the correlations and predicting the ice loads (Kotilainen et al., 2017; Kujala et al., 2019; Bekker et al., 2019). Parameters related to ship operations and ice conditions are considered to contribute to the ice loading magnitude. Studies have shown that the ice thickness, as well as ice concentration, has an increasing effect on the ice load magnitude (see e.g. Hänninen et al., 2001; Suominen et al., 2015; Kotilainen et al., 2017; Ritch, 2008). In addition, researches also show that highest loads have been measured at intermediate speeds on many occasions (see e.g. St. John and Minnick, 1995; Hänninen et al., 2001; Suominen et al., 2015). However, there are relatively less study specifically on multiyear ice or ramming cases to understand what this particular and potentially dangerous ice condition will cause to the ship local structure. The rare ice condition and limited ramming cases with multi-source measurement facilities available onboard may be the reason of

such studies. During the 7th voyage to Antarctica for S.A. Agulhas II, a polar research vessel, the situation of ramming into a multiyear thick ice floe occurred and lasted for 3 days. This paper bases on the data collected from this ramming period.

S.A. Agulhas II was chartered for Weddell Sea Expedition 2019 during 1st January to 15th February. The overarching objectives of the Weddell Sea Expedition are to undertake scientific research program in the Larsen C Ice Shelf region and attempt to locate and undertake a marine archaeological survey of the historic wreck of Sir Ernest Shackleton's ship Endurance, which sank in the western Weddell Sea in 1915. Therefore, one of the important devices in the expedition is the AUV (Automatic Underwater Vehicle). However, the AUV went missing under a big multiyear ice floe during the sea trial, when it was applied to map the bottom of the ice floe. The ship then had to carve the ice floe intentionally to find the missing AUV. Figure 1 shows the general route from 6th December 2018 to 14th March 2019. The intentional ship-ice ramming happened in the period 16th to 18th January 2019 as shown in the left up corner in Figure 1. Figure 2 shows the satellite image of the ice floe during the carving period.
This paper focuses on this particular case in the Antarctic Weddell Sea, and aims to provide insights into following research questions:

1) what is the ice loads on the ship bow when ramming into thick multiyear ice based on the installed measurement system;
2) what are the leading factors affecting the ice loads when the ship rams into thick ice floe, and what operational actions can be performed to avoid high loads if the ship is colliding with unavoidable huge multiyear ice during normal navigation.

Following this introduction, section 2 focuses on the description of methodology and data. Section 3 presents the results. Section 4 discusses and Section 5 concludes.

Figure 1. General route during the whole expedition and the ship track during the carving of multiyear ice.

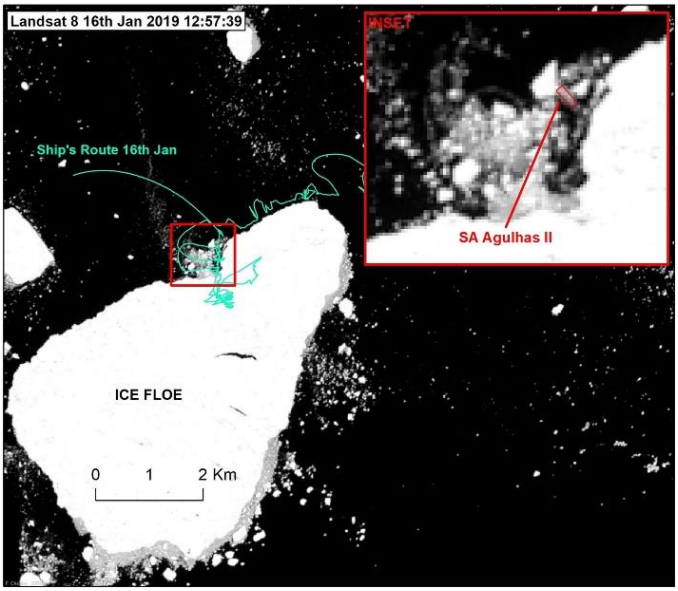

Figure 2. Satellite image during the carving. The image is processed by Scott Polar Institute during Weddell Sea Expedition 2019.

2 DATA AND METHODOLOGY

2.1 *Ship and instrumentation*

The construction of the Polar Supply and Research Vessel (PSRV) S.A. Agulhas II was completed in April 2012. The ship was built to Polar ice class PC 5 (IACS, 2016) and the strength of the hull in accordance with DNV ICE-10 (DNV, 2012). The main dimensions of the ship are presented in Table 2.

Table 1. The main dimensions of the ship

Parameter	Value	Unit
Length, bpp.	121.8	[m]
Breadth, mould.	21.7	[m]
Draught, design	7.65	[m]
Deadweight at design displacement	5 000	[t]
Service speed	14.0	[kn]

Three areas of the ship hull - the bow, bow shoulder and stern shoulder - were instrumented with strain gauges for the ice loads on the ship hull measurements. Two frames at the bow, three frames at the bow shoulder and four frames at the stern shoulder were instrumented for the ice load measurements. Furthermore, strain gauges were mounted on the hull plating for strain measurements: two gauges at the bow, two at the bow shoulder, and six at the stern shoulder. The instrumentation of the ship is presented in Figure 3.

The strains were measured with a frequency of 200 Hz during the whole voyage. In addition, cameras are installed, which are distinguished as: i) ice thickness camera, which is a stereo camera installed on the starboard side on the fifth deck, under the bridge; ii) ice load cameras, which are used to monitor the ice breaking patterns at the locations of strain gauges; iii) ice condition camera, on the top of the ship, which is used to record the ice conditions dur-

ing the ship operation. Meanwhile, the visual observation of the ice conditions is conducted in the bridge. Two IMUs (Inertial Measurement Unit) are also installed on the ship as indicated in Figure 3 to record the motions of the ship. A central measurement unit also gives the ship navigation data and machine control data in addition to the recorded strains.

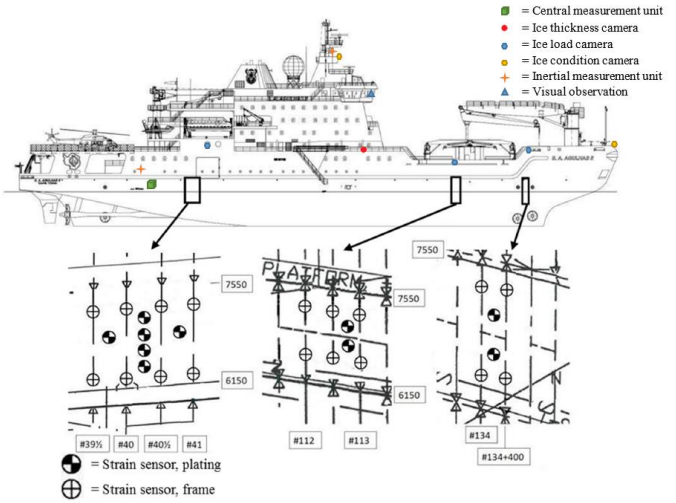

Figure 3. The instrumentation of the ship.

2.2 *Data and processing*

The data used for this paper are based on the ice load data, navigation data, machine control data and ice condition camera data. The dataset is used to extract following parameters: SOG (Speed Over Ground), rudder angle, power, ramming angle, and ice condition. These parameters are considered to relate to ramming-induced ice loads. Figure 4 shows the process to get the combined data matrix of relevant parameters. First, the ice loads need to be calculated from the raw data. The ice loads on the ship hull were determined from the measured shear strains on the instrumented frames at the bow, bow shoulder and stern shoulder. The ice loads were calculated with following equation:

$$F=a\cdot\Delta\gamma \quad (1)$$

where 'a' is the stiffness matrix and $\Delta\gamma$ is the calculated change in shear strain between the two sensors on one frame. According to Suominen et al. (2015a), the stiffness matrices for the bow shoulder and stern shoulder were determined from the calibration pulls and for the bow the matrix was estimated from the finite Element model.

Secondly, the five-minute maximum ice load is extracted from the ice load data for further analysis. Meanwhile, a criterion where only loads larger than 100 KN are retained is applied to further filter the data so that only relatively large ice load events will be further analyzed. After identifying the targeted ice load event, the recorded time of the maximum ice load event will be used as index to find the corresponding SOG (Speed Over Ground), power, rudder angle, ice condition, and ramming angle in their corresponding dataset. In the end, the matrix of relevant parameters are is formed for further analysis.

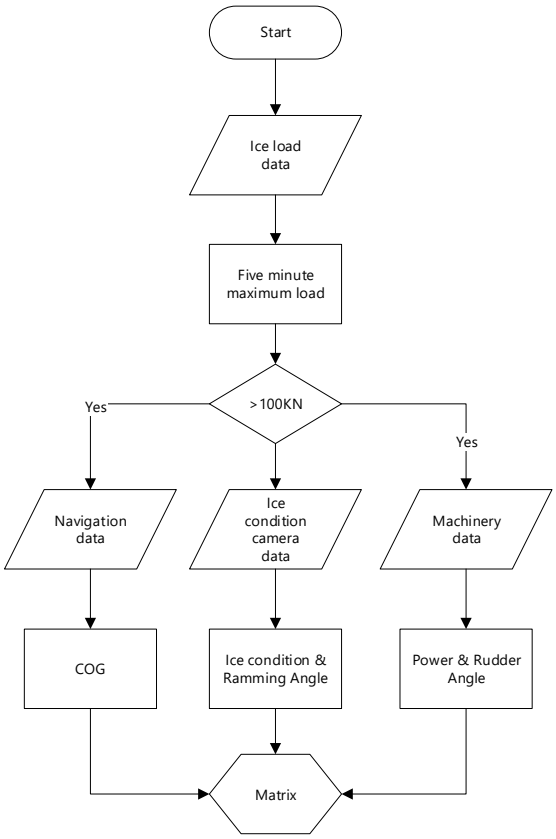

Figure 4. Data processing flowchart.

In addition, ice properties of the ice floe are also measured by ice field work, e.g. ice coring and bending, as background knowledge to understand the ice loads. The results of these measurements are shown in Section 3.3.1.

2.3 *Analysis method*

After obtaining the data matrix, a statistical method, Bayesian Network (BN), is applied to analyze the data. BNs are relatively widely used tools for risk modeling and have been applied many fields (Fenton & Neil, 2012), including maritime risk analysis(Lim et al., 2018; Aps et al., 2009; Helle et al., 2015).

In mathematical terms, BNs represent a class of probabilistic graphical models, defined as a pair $\Delta=\{G(V,A),P\}$ (Koller & Friedman, 2009), where G(V,A) is the graphical component and P the probabilistic component of the model. G(V,A) is in the form of a directed acyclic graph (DAG), where the nodes represent the variables $V=\{V_1,\ldots,V_n\}$ and the arcs (A) represent the conditional (in)dependence relationships between these. P consists of a set of conditional probability tables (CPTs) $P(V_i|Pa(V_i))$ for each variable V_i, $i=1,\ldots,n$ in the network. $Pa(V_i)$ signifies the set of parents of V_i in G: $Pa(V_i)=\{Y\in V|(Y,V_i)\}$. A BN encodes a factorization

of the joint probability distribution (JDP) over all variables in V (Goerlandt and Montewka, 2015; Lu et al., 2019):

$$P(V)=\prod_{i=1}^{n}P\left(V_i \mid \boldsymbol{Pa}\left(V_i\right)\right) \tag{2}$$

3 RESULTS

3.1 *Ice property*

Ice properties were measured from the ice floe so that a better understanding is obtained of what kind of ice the ship was ramming. Figure 5 shows the temperature, salinity and, density measurements from a 5.2 m ice core. In general, the temperature decreases from 0 to -1.6 ℃ along the depth. The salinity rises from 1‰ to 6‰ with fluctuations and the density ranges from around 800 to 900 kg/m^3 from top to bottom of the ice core.

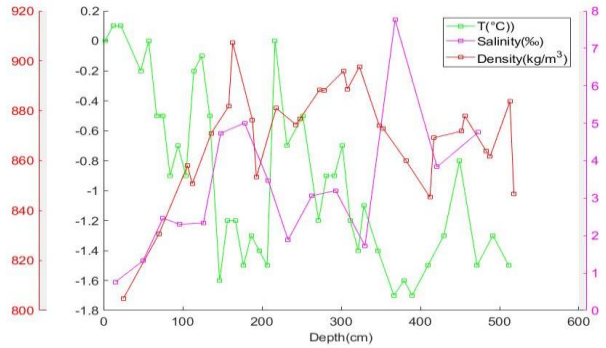

Figure 5. Temperature, salinity and density measurements along ice core.

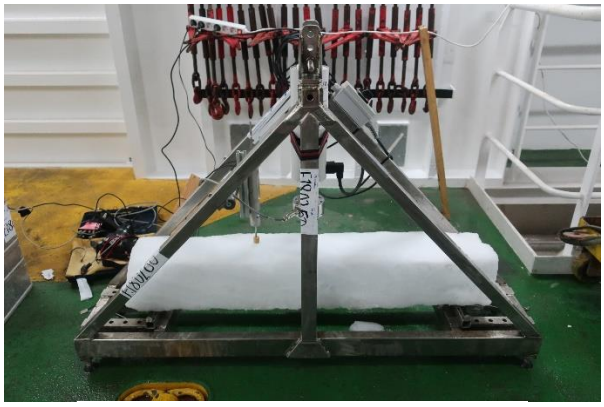

		s2	s1
	s4	s3	

Figure 6. Ice bending test and ice sample locations in the ice block.

The ice flexure strength was obtained by conducting three-point bending tests from an ice block near the top part of the ice floe, as shown in Figure 6. The beam was simply supported on both ends by the steel frame and was loaded downwards from the middle. The force needed to break the beam was measured with a load sensor, see Figure 6. The bending strength was then determined with an equation:

$$\sigma_f=\frac{3}{4}\cdot\frac{(2F+G)\cdot L}{b\cdot h^2} \tag{3}$$

where F = the measured maximum force, G = gravity force $= b\times h\times L\times\rho\times g$, L = support span, b = sample width, h = sample height, ρ = ice density determined from the density measurements, g = gravity acceleration.

Table 2 shows the calculated flexure strengths of the ice samples. As shown in Figure 6, sample s1 and s2 are from the top layer; s3 and s4 are in the next layer of the ice block. There is no obvious trends of flexure strength change between the layers. The flexure strength measured is around 250 kPa.

Table 2. Ice flexure strength and other relevant parameters from the tested samples

Sample	ρ (kg/m3)	σ (kPa)
s1	833.6	242.7
s2	821.7	256.7
s3	808.5	277.4
s4	844.3	221.0

3.2 *Ice loads on ship bow*

The ramming from the ice floe mainly happened on the ship bow. Therefore, the ice loads on ship bow shoulder and stern shoulder are mostly zero, whereas only the ship bow frames experience big impacts from the ramming with the ice floe.

Five-minute maximum ice loads on two frames at the ship bow are shown in Figure 7, without any filtering. It is seen that the ice load varies significantly in each five-minute period, which means each ramming results into a quite different ice load, even the ship is ramming the same ice floe. Most of the ice loads are under 500 KN; whereas there are nine and eleven ramming induced ice loads between 500 to 1000 KN on Frame 134 and Frame 134+400mm respectively. Only one ramming caused ice load over 1000 KN on both frames. However, they happened in different ramming events. On Frame 134, the maximum ice load happened at 00:48:26.8, 18.01.2019. The load reached 1264.3 KN, while measured ice load on Frame 134+400mm is 331.8 KN. The maximum ice load on Frame 134+400mm was 1254 KN, occurred at 09:53:2.5, 16.01.2019 and the load on Frame 134 was almost zero. Therefore, the ice load seems to be a very local phenomenon from the measured results.

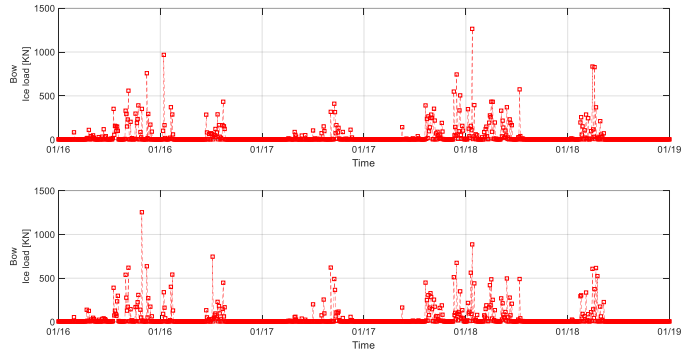

Figure 7. Five-minute maximum ice load history during ramming.

3.3 *Correlation between operational parameters and ice loads*

To further analyze and correlate potentially relevant factors, the subsequent analysis focuses on the relatively large ship-ice ramming. In particular, ice loads larger than 100 KN are selected and the ship operational parameters at the nearest time of those loads are associated with these loads. Figure 8 and 9 shows correlation matrices of the ice loads and ship operational parameters: SOG, port rudder angle, starboard rudder angle, port motor power, and starboard motor power. From the results, no obvious pairwise correlations between ice loads and operational parameters can be observed on both frames as the correlation factor is too small. The only obvious confirmation is that the correlation factors between starboard rudder angle and port rudder angle are equal to one. The same trend can be observed between starboard motor power and port motor power. They have correlation factor close to one. This indicates that rudder and power from the starboard and port sides are applied synchronously in the ramming cases. Therefore, only port rudder angle will be used in further analysis and superimposed power from port and starboard side will appear instead of individual one.

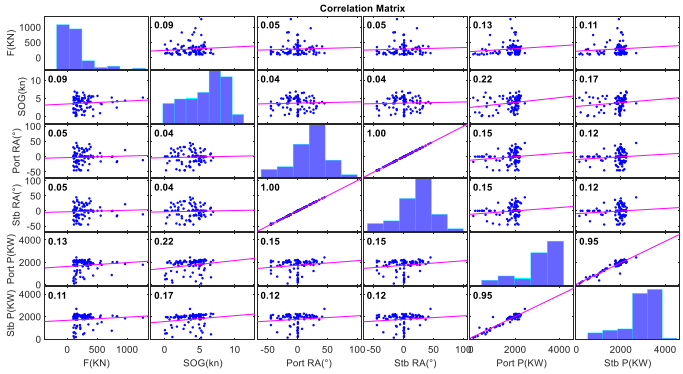

Figure 8. Correlation among parameters on Frame.

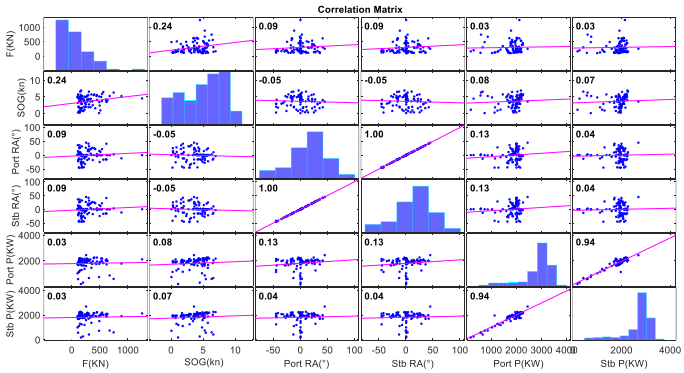

Figure 9. Correlation among parameters on Frame 134+400mm.

The selection of ice loads larger than 200 KN is conducted to focus on relatively more severe ramming cases. However, similar as Figure 8 and 9, the correlation matrix does not give any obvious implications. Figure 10 presents scatter plots of Ice loads F, which are larger than 200 KN, together with SOG (V), portside rudder angle (RA) and total motor power (P). Most significant ramming happened on 16th and 18th January. The power stays quite high usually and the speed varies more than the power. Meanwhile, the ice loads are also in a wide range. The rudder angles are more on zero and starboard direction.

Table 3 shows the cases where the ice loads are greater than 800 KN on both frames. From these high load cases, some common features can be observed, i.e. powers and speeds are relatively high and the port direction rudder controls are more likely to cause these high ice loads. The angles are not too large, but they can lead the starboard side bow to face more directly to the ice. In those cases, the ice impacts are more perpendicular to the ship bow frames and are more likely to result in high loads on the instrumented frames.

Table 3. Cases of ice loads larger than 800 KN

Time	F(KN)	V(kn)	RA(°)	P(KW)
2019.1.16 12:25:10	967	4.4	21.9	3696
2019.1.18 00:48:26	1264	5.2	-11.4	3696
2019.1.18 14:57:43	834	4.2	-14.9	4068
2019.1.18 15:13:03	827	2.4	-17.5	3978
2019.1.16 09:53:02	1254	4.5	0.14	4256
2019.1.18 00:48:27	886	5.2	-11.4	3699

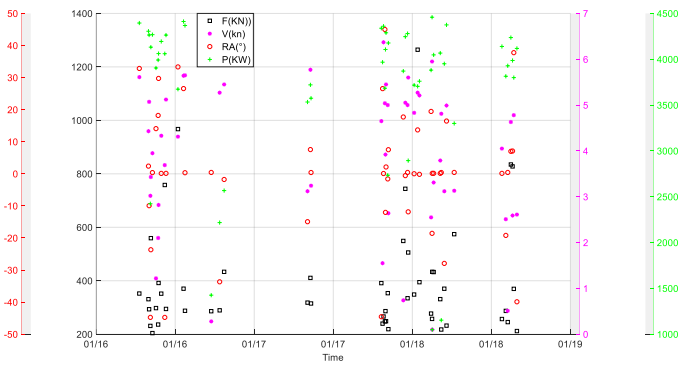

Figure 10. Scatter distribution of ice loads and operational parameters on Frame 134. Unites of the axes are shown in the legend.

3.4 *Statistical model analysis of the parameters and ice loads*

The focus until now are on operational parameters, however, ice related parameters and the ramming angles are also considered as possibly relevant factors. Therefore, a more comprehensive dataset is created and analyzed in this section.

Usually, ice concentration, thickness, strength (compression and flexure strength) are the representative parameters of ice (Suominen, 2018). The ice concentration is 100% in this case, so it is not relevant in this case study. The ice thickness and flexure strength are measured from this ice floe as described in section 3.1. However, the measured ice thickness and flexure strength are only from one specific site from the ice floe. During the ramming, the ship is carving the ice continuously at different locations, therefore the two measured parameters are not sufficient to represent the ice the ship is carving, i.e. they cannot be directly linked with the measured ice loads. Instead, they can be used just as a reference and background knowledge for this ramming situation, not in the parameter analysis. Therefore, a qualitative approach is applied, i.e. observing the encountered ice from ice condition camera and using number 1-3 to define ice condition. 1-3 stands for broken ice, level ice and ridged ice respectively, referring to the 5.2 m ice thickness and relevant ice properties. Meanwhile, ramming angles are deduced by calculating relative angles between ice edge and ship starboard hull. Figure 11 shows the ice conditions in the maximum ice load case from different cameras. The ice condition is defined as 3.

With more complete information of the ramming cases, a statistical Bayesian Network model is considered to use to learn the parameters and give implications. First, all the parameters on frame 134 are discretized. Considering the existing ice condition definition, the other parameters are also discretized into three levels, except rudder angle, as shown in Table 4.

Table 4. Discretization of the parameters

Parameter	Discretization
V (kn)	low [1,2]; medium [2,4]; high [4+]
RA (°)	port large [-45,-22.5]; port small [-22.5,0]; stb small [0,22.5]; stb large [22.5,45]
P (KW)	low [0,1500]; medium []1500,3500]; high [3500+]
ICE	broken [1]; level [2]; ridge [3]
CA (°)	stb small [0,45]; stb medium [45,90]; port [90,360]
IL (KN)	low [0,300]; medium [300,800]; high [800+]

V – Speed; RA – Rudder Angle; P – Power; ICE – Ice Condition; CA – Ramming Angle; IL – Ice Load; stb – starboard

Figure 11. Ice conditions in the maximum ice load case.

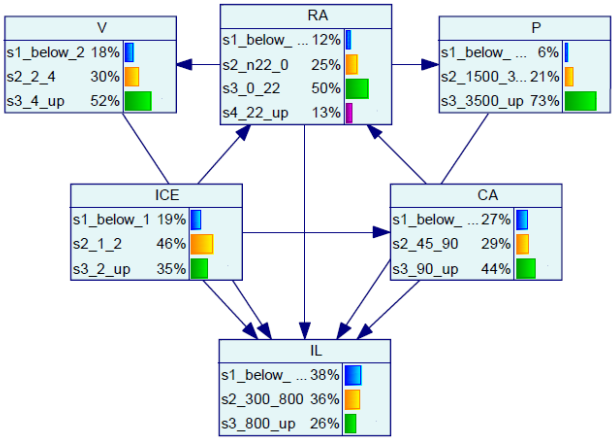

Figure 12. Bayesian network model.

After the discretization, the network is learnt from the data by algorithm in GeNIe under the instructed structure, i.e. all the parameters are indicated to affect the ice load. Figure 12 is the Bayesian network learnt from the data. It is seen that all the parameters are contributing to ice loads as instructed. In addition, the structure learnt from the data indicates that

the ice condition influences the ramming angle and rudder angle. There is no direct link between ship speed and ice condition learnt from the data. However, rudder angle is under the influence of the ice condition and ramming angle and it links motor power and ship speed.

Table 5 shows the probabilities of ice load states by making each state of corresponding parameter as evidence. If the focus is only on the high load, from the results, it is seen that the medium speed range has a higher probability to result in high loads. However, the difference between the probabilities is quite small, so the significance is questionable due to the relatively limited dataset. Port rudder angles are more likely to cause high loads in general. Small port rudder angles have a relatively high probability for high loads. Similarly, for ramming angle, starboard angles are more likely to induce high loads. These can be explained as the strain gauge sensors are in the starboard bow side. These directions may cause more perpendicular forces. In addition, the broken and ridge ice conditions have a relatively high probability of causing high loads. It should be noted that the ice loads refer only to this specific ice floe or similar ice floe or ice conditions as described in the ice property part. Generally, in this kind of case, the probability of having local high ice loads on the bow hull is between 20% to 35%, if the ship is ramming into a multiyear thick ice condition.

Table 5. Probabilities of the Ice loads by applying each state of parameters as evidence. The numbers are in percentage.

IL	V			RA			ICE				CA		
	L	M	H	PL	PS	SS	SL	BI	LI	RI	SS	SM	P
L	43	34	38	39	36	41	33	30	45	33	33	32	45
M	32	38	36	33	33	37	41	40	32	39	39	39	32
H	24	27	25	28	31	22	27	30	22	28	28	29	22

4 DISCUSSION

4.1 *Uncertainty caused by time difference*

The ice load is the load measured on the frame, so the local ice load happens in a very short time, within 1 second. Even though the aim is to find the exact time of all the parameters at the maximum ice load time, the frequency difference among ice load measurement (200HZ), navigational data (1HZ) and machine control data (0.5HZ) leads to challenges in exactly matching the data. By investigating the matching time from maximum ice loads and machine control data, it is found that most time differences between maximum load and machine control data are less than 1 second, only four cases are beyond 1 second, but within 2 seconds. All the navigational data are within 0.5 seconds difference comparing to the maximum load time. The time differences are in the smallest possible difference range, however, the time difference still cause uncertainties when correlating all the parameters to the same time.

4.2 *Uncertainty caused by the thick ice*

The ice thickness was quite large; therefore, the ice was broken by the weight of the ship in many cases. During the ramming period, it was observed that the ship bow would be lifted onto the very thick ice if the speed were relatively large. This may explain that medium speeds seems more likely to cause high local loads on the frame as if the speed is too large, the ship bow and instrumented frame may be lifted out of ice. In addition, the breaking pattern of the ice also has effect on the local ice loads, which can be further analyzed to understand better in the ice loads.

5 CONCLUSION

This paper analyzed the ramming induced ice loads between ship bow and thick multiyear ice. The ramming between the ship bow and the thick multiyear ice floe can cause various ice loads on the side bow in this case study. Most of the ice loads are under 500 KN; whereas there are nine and eleven ramming induced ice loads between 500 to 1000 KN. Only one ramming caused ice load over 1000 KN on both frames, up to around 1259 KN. In addition, the peak ice loads are found to occur very locally.

It is hard to find clear corrections between the external parameters and ice loads directly, which proved also ice loads are not determined by certain parameter purely in multiyear ice ramming scenarios. A statistical Bayesian Network model is created based on the parameters and data. The probability of having local high ice loads on the bow hull is between 20% to 35% generally. Medium speed also indicates relatively high ice loads in multiyear ramming cases, which is identical with the other research findings in general ship-ice interaction cases (St. John and Minnick, 1995; Hänninen et al., 2001; Suominen et al., 2015). The broken and ridge ice conditions have a relatively high probability of causing high loads. This should be noticed in the practical operation as the broken ice may be ignored. Small port rudder angles, as well as the starboard ramming angles, are more likely to cause high loads on starboard bow side when the ship rams multiyear ice floe.

ACKNOWLEDGEMENTS

The work was funded by the Lloyd's Register Foundation (the grant for Centre of Excellence for Arctic Shipping and Operations). The Lloyd's Register Foundation helps to protect life and property by supporting engineering-related education, public engagement and the application of research. The author would also like to thank Weddell Sea Expedition 2019, the dataset are obtained during the expedition. Especially Stellenbosch University team, An-

nie Bekker, Christof M. van Zijl, James-John Mattheee, who helped a lot on the ice property measurement.

REFERENCES

Bekker, A., Lu, L., van Zijl, C.M., Mattthee, J.J., Kujala, P., 2019. Correlation between bow ice loads and operational responses during ice navigation in the Weddell Sea. Proceedings of the 25th International Conference on Port and Ocean Engineering under Arctic Conditions, June 9-13, 2019, Delft, The Netherlands

Bridges, R., Riska, K., Lu, L., du-Couedic-du-Kererant, M., Aubert, J.M., 2018. A study on the specification of minimum design air temperature for ships and offshore structures. Ocean Eng., 160 (2018), pp. 478-489

DNV, 2012. Rules for classification of ships Part 5 Chapter 1, Det Norske Veritas, Oslo, Norway, 2012

Ehlers, S., Cheng, F., Kuehnlein, W., Jordaan, I., Kujala, P., Luo, Y., Riska, K., Sirkar, J., Oh, Y., Terai, K., Valkonen, J., Ralph, F., 2015. 19th Int. Ship and Offshore Structures Congress Committee V.6 Arctic Technology, Cascais, Portugal, September 7-10, 2015, pp. 770-816.

Frédéric, L., 2011. Arctic shipping routes : From the Panama myth to reality. International Journal: Canada's J. Glob. Policy Anal. 66(4), 793–808.

Goerlandt, F., Montewka, J., 2015, A framework for risk analysis of maritime transportation systems: a case study for oil spill from tankers in a ship–ship collision. Saf. Sci., 76 (2015), pp. 42-66, 10.1016/J.SSCI.2015.02.009

Hänninen, S., Lensu, M., Riska, K., 2001. Analysis of the Ice Load Measurements during USCGC Healy Ice Trials, Spring 2000. Helsinki University of Technology, Ship Laboratory, Report M-265, Espoo, Finland.

IACS, 2016. International Association of Classification Societies. Requirements concerning POLAR CLASS, 2016

Jordaan, I. J., Maes, M. A., Brown, P. W., Hermans, I. P., 1993. Probabilistic Analysis of Local Ice Pressures. ASME Journal of Offshore Mechanics and Arctic Engineering 1993;115:83-89.

Jordaan, I., Bruce, J., Masterson, D., Frederking, R. 2010. Local ice pressures for multi year ice accounting for exposure. J. Cold Reg. Sci. Technol., 61 (2010), pp. 97-106

Kendrick, A., Daley, C., 2011. Structural challenges faced by Arctic ships, Ship Structure Committee, Report No. 461.

Kujala, P., 1994. On the Statistics of Ice Loads on Ship Hull in the Baltic. Doctoral Thesis, Helsinki University of Technology, Ship Laboratory, Acta Polytechnica Scandinavica Mechanical Engineering Series No. 116, 98 pp

Kujala, P., Jiang, Z., Li, F., Lu, L., 2019. Long term prediction of local ice loads on the hull of S.A. Agulhas II. Proceedings of the 25th International Conference on Port and Ocean Engineering under Arctic Conditions, June 9-13, 2019, Delft, The Netherlands

Kotilainen, M., Vanhatalo, J., Suominen, M., Kujala, P., 2017. Predicting ice-induced load amplitudes on ship bow conditional on ice thickness and ship speed in the Baltic Sea. Cold Regions Science and Technology 2017;135:116-126.

Lu, L., Goerlandt, F., Banda, O.A.V., Kujala, P., Höglund, A., Arneborg, L., 2019. A bayesian network risk model for assessing oil spill recovery effectiveness in the ice-covered northern Baltic Sea. Mar. Pollut. Bull., 139 (2019), pp. 440-458

Ritch, R., 2008. First Year Hull-Ice Interaction Loads Measured on the Louis S. St-Laurent During the 1995 Gulf of St. Lawrence Trials, the 8th International Conference and Exhibition on Performance of Ships and Structures in Ice, ICETECH 08, Calgary, Alberta, Canada, July 20-23, 2008.

St. John, J., Minnick, P., 1995. Ice Load Impact Study on the National Science Foundation's Research Vessel Nathaniel B. Palmer, Ship Structure Committee, Report No. 376.

Suominen, M., Romanoff, J., Remes, H., Kujala, P., 2015a. The determination of ice-induced loads on ship hull from shear strain measurements. Proceedings of the 5th International Conference on Marine Structures (MARSTRUCT). Southampton, UK, March 25-27, 2015

Suominen, M., Kujala, P., Kotilainen, M., 2015. The encountered extreme events and predicted maximum ice-induced loads on the ship hull in the Southern Ocean. 34th Int. Conf. on Ocean, Offshore and Arctic Engineering, St. John's, Newfoundland, Canada, May 31-June 5, 2015.

Suominen, M. 2018. Uncertainty and variation in measured ice-induced loads on a ship hull. Doctoral Thesis. Aalto University publication series. Helsinki, Finland, P149

Taylor RS, Jordaan IJ, Li C, Sudom D. Local Design Pressures for Structures in Ice: Analysis of Full-Scale Data. ASME. J. Offshore Mech. Arct. Eng. 2010;132(3):031502-031502-7. doi:10.1115/1.4000504